Treatment and Resource Recovery

Coupling Filter-Based Thermal Desorption Chemical Ionization Mass Spectrometry with Liquid Chromatography/Electrospray Ionization Mass Spectrometry for Molecular Analysis of Secondary Organic Aerosol

Yuanlong Huang, Christopher M Kenseth, Nathan F. Dalleska, and John H. Seinfeld

Environ. Sci. Technol., **Just Accepted Manuscript** • DOI: 10.1021/acs.est.0c01779 • Publication Date (Web): 12 Jun 2020

Coupling Filter-Based Thermal Desorption Chemical Ionization Mass Spectrometry with Liquid Chromatography/Electrospray Ionization Mass Spectrometry for Molecular Analysis of Secondary Organic Aerosol

Yuanlong Huang,[†] Christopher M. Kenseth,[‡] Nathan F. Dalleska,[†] and John H. Seinfeld[*,‡,¶]

[†]*Division of Geological and Planetary Sciences, California Institute of Technology, Pasadena, CA, USA, 91125*

[‡]*Division of Chemistry and Chemical Engineering, California Institute of Technology, Pasadena, CA, USA, 91125*

[¶]*Division of Engineering and Applied Science, California Institute of Technology, Pasadena, CA, USA, 91125*

E-mail: seinfeld@caltech.edu

Phone: +1 626 395 4635. Fax: +1 626 568 8743

Abstract

Filter-based thermal desorption (F-TD) techniques, such as the filter inlet for gases and aerosols (FIGAERO), are widely employed to investigate the molecular composition and physicochemical properties of secondary organic aerosol (SOA). Here, we

introduce an enhanced capability of F-TD through combination of a customized F-TD inlet with chemical ionization mass spectrometry (CIMS) and ultra-performance liquid chromatography/ electrospray ionization mass spectrometry (UPLC/ESI-MS). The utility of F-TD/CIMS + UPLC/ESI-MS is demonstrated by application to α-pinene ozonolysis SOA, for which increased filter aerosol mass loading is shown to slow the evaporation rates of deposited compounds. Evidence for oligomer decomposition producing multi-mode F-TD/CIMS thermograms is provided by measurement of the mass fraction remaining (MFR) of monomeric and dimeric α-pinene oxidation products on the filter via UPLC/ESI-MS. In-situ evaporation of aerosol particles suggests that α-pinene-derived hydroperoxides are thermally labile; thus, analysis of particle-phase (hydro)peroxides via F-TD may not be appropriate. A synthesized pinene-derived dimer ester ($C_{20}H_{32}O_5$) is found to be thermally stable up to 200 °C, whereas particle-phase dimers ($C_{19}H_{30}O_5$) are observed to form during F-TD analysis via thermally induced condensation of synthesized pinene-derived alcohols and diacids. The complementary F-TD/CIMS + UPLC/ESI-MS method offers previously inaccessible insight into the molecular composition and thermal desorption behavior of SOA that both clarifies and expands on analysis via traditional F-TD techniques.

Introduction

Analysis of secondary organic aerosol (SOA) formation includes consideration of gas-phase chemistry, multi-phase transport,[1] particle phase state (or viscosity),[2] and particle-phase reactions (e.g., oligomerization). No single instrument exists that can interrogate all these processes. A significant challenge to the molecular-level detection of SOA constituents is the fact that aerosol particles comprise only a small amount of mass, yet generally contain an extensive array of diverse compounds. Moveover, the nature of SOA generally requires pre-treatment (e.g., thermal desorption, extraction, charging, etc.) before analysis of particle physicochemical properties.

Heat-induced evaporation of particles, as a pre-treatment process, has long been employed to investigate aerosol volatility, as well as particle-phase composition[3–5]. Two common particle-evaporation techniques include: (1) detection of the vapors coming off the particles (e.g., with a mass spectrometer[6–8]), and (2) removing the vapors with adsorptive materials (e.g., with a thermodenuder[9,10]) to determine the mass fraction remaining (MFR) in the particle phase after evaporation. These two approaches can provide complementary understanding of SOA chemical properties if one can simultaneously analyze both the vapors from the particles as well as the mass remaining in the particles.

To address the minute amount of single-particle mass, particles are routinely collected on filters or impactors[11,12] and analysis is focused on the concentrated material. A recently developed technique, the filter inlet for gases and aerosols (FIGAERO),[13] is now widely employed to investigate SOA composition. The details of FIGAERO operation, which leverages filter-based evaporation to detect both gas- and particle-phase components in a semi-continuous mode, are described extensively elsewhere.[14–17]

Application of filter-based evaporation of aerosol-phase compounds upon heating has significantly advanced analysis of SOA composition across a wide range of molecular volatilities. Nevertheless, some intrinsic properties of this method introduce uncertainties into the data analysis. First, the temperature at which the chemical ionization mass spectrometer (CIMS) detects the maximum ion signal during thermal desorption (so-called $T_{\max}$) for a pure compound can differ as a function of the analyte matrix (i.e., pure compound vs. SOA sample).[13] This results because 1. (semi-)solid particle phase states determined by aerosol composition may retard the evaporation,[17] 2. increasing aerosol mass loading on the filter[18] may limit inter-layer particle-phase diffusion, and 3. the complexity of SOA may induce stronger non-covalent H-bonding between the compound of interest and other SOA constituents as compared to those of the pure compound.[19] Second, temperature ramping to separate particle-phase components based on molecular volatility can lead to thermal decomposition of larger molecules or oligomerization in the condensed phase with poorly con-

strained transformation rates.[20,21] Third, owing to the relatively large surface area of filters in F-TD, evaporated molecules can interact with the filter (e.g., adsorption and desorption) before entering the CIMS. Schobesberger et al.[5] developed a comprehensive model framework to explain observed thermograms (CIMS signal vs. temperature) for different compounds that incorporates the effect of the filter itself and is based on temperature-dependent reversible oligomerization between monomers and oligomers and irreversible thermal decomposition.

Owing to these issues associated with thermal-induced evaporation of aerosols, interpretation of data derived from thermal desorption measurements and direct comparison between studies are difficult. Alternatively, another widely used, comparatively mild, method to pretreat aerosol samples is extraction followed by electrospray ionization (ESI), often coupled with liquid chromatography (LC). It is noted, however, that the extraction efficiency of the condensed-phase compound depends on the polarity of the solvent.[22] Furthermore, ESI efficiencies have been shown to depend strongly on molecular structure.[23]

Here, we introduce and demonstrate a complementary capability of filter-based thermal desorption (F-TD) by combining a customized inlet system, the key feature of FIGAERO, with CIMS and off-line ultra-performance liquid chromatography/electrospray ionization mass spectrometry (UPLC/ESI-MS). The F-TD inlet processes the filter sample with a conventional procedure (ramp to a temperature setpoint and hold), from which one obtains thermograms of evaporating species via CIMS, while UPLC/ESI-MS provides complementary information about the components remaining on the filter after evaporation under a range of temperatures. The combination of F-TD/CIMS + UPLC/ESI-MS enables a more comprehensive analysis of aerosol molecular composition and volatility than that afforded by traditional thermal desorption techniques. With F-TD/CIMS + UPLC/ESI-MS, we seek to: (1) provide direct evidence for the role of thermal decomposition in producing multi-mode thermograms; (2) demonstrate that the amount of aerosol mass deposited on the filter affects the performance of thermal desorption in terms of both evaporation fluxes and the MFR in the particle phase, and (3) explore the thermal stability and reactivity of typical aerosol

oxidation products.

Experimental

Filter-Based Thermal Desorption System

A custom F-TD inlet system was developed for the Caltech CIMS.[24] The basic operating principles of the F-TD inlet follow those of the FIGAERO.[13] The F-TD inlet scheme and a detailed comparison with the FIGAERO can be found in the Supplementary Material (SI.I and Fig. S1a). Evaluation of the performance of the F-TD system is described in SI.II. Briefly, the F-TD inlet comprises three parts: N_2 flow control system, heating system, and filter holder. The main N_2 flow is set at 2 LPM by a mass flow controller (Horiba, SEC-4400MC), while a critical orifice extracts 200 ccm N_2 from a bypass flow open to the room air; together these flows maintain the pressure in the ion-molecule reaction (IMR) chamber at 26.6 Torr. The heating tube of 8-inch length and 3/8-inch OD stainless steel is surrounded by ultra-high temperature heating tape (Omega, STH051-020). The heating process involves a ramping controller (Watlow, F4SH-CKA0-01RG) and two K-type thermocouple probes (PerfectPrime) that monitor temperature: Probe 1 (TL0260) is positioned above the filter and provides the feedback to the ramping controller, while Probe 2 (TL0700) is twined with the heating tape. The probes are connected to an Arduino board (UNO Rev3), and real-time data are recorded by a customized program in MATLAB (R2010) through a serial cable. The stainless steel filter holder is customized for 25 mm diameter filters with a hole for Probe 1. A stainless steel porous disc pre-treated by FluoroPel (Cytonix, 801A) is used to support the filter. The essential difference between the F-TD inlet and that of FIGAERO is the pressure to which the filter is exposed: 26.6 Torr vs. ambient pressure. The pressure of the F-TD, however, is still much higher than the vapor pressure of typical SOA oxidation products, thus having limited impact on their evaporation behavior compared to that in the FIGAERO (see explanation in SI.I). Vapor wall loss is also minimized during transportation

from the filter to the IMR immediately below.

CF_3O^--CIMS

The quadrupole CIMS (nominal m/z) uses CF_3O^- as the reagent ion, which has high selectivity for multifunctional compounds and hydroperoxides (ROOH).[24] CF_3O^- is generated by exposing a flow of 10 ppmv CF_3OOCF_3 in N_2 to a radioactive ^{210}Po source. In the IMR chamber, which is maintained at 26.6 Torr, the analytes M can be ionized through: clustering ($M \cdot CF_3O^-$), F^- transfer ($HF \cdot M_{-H}{}^-$), or proton transfer ($M_{-H}{}^-$) channels. The quadrupole MS was operated in scanning mode (m/z 50 - 400), with a scan rate of $\sim$ 1.5 s. Details concerning the design and characterization of CF_3O^--CIMS can be found elsewhere.[25,26]

Filter Sample Collection and Pre-treatment

Analysis of α-pinene ozonolysis SOA, an extensively investigated system in the steady-state Caltech photo-oxidation flow tube reactor (CPOT)[27] consisting predominantly of monomers (C_{7-10}) and dimers (C_{14-20}), was used to evaluate the methodology. A continuous flow of α-pinene (Airgas, 20 ppm in N_2) at 75 ccm was mixed with 5 LPM purified air (generated by Parker 75-62NA), yielding a steady-state α-pinene concentration of $\sim$300 ppb with an average CPOT residence time of 10 min. O_3 was maintained at a mixing ratio of 1 ppm by adjusting the flow rate of purified air through an ozone generator (AnalytikJena, 97-0067-01). The high concentrations of α-pinene and O_3 in CPOT were used to generate sufficient SOA mass for further analysis. Neither seed aerosol nor OH scavenger was used. Relative humidity was $< 1\%$ and temperature was maintained at 25 ± 0.2 °C. The CPOT outlet flow was pulled through an activated charcoal denuder that efficiently removed gas-phase organic components and O_3 before collection on Teflon filters (TF 1000, 1 μm pore size, Pall Corp.). The CPOT experimental setup is shown in Fig. S4.

To evaluate the extent to which the amount of aerosol mass on the filter might bias the data analysis, filters were collected for either $\sim$ 30 or $\sim$ 300 min, corresponding to

estimated organic aerosol mass depositions of ~ 1 and ~ 10 μg cm^{-2}, respectively (assuming an effective SOA density of 1.2 g cm^{-3} and an effective filter collection radius of 1 cm). Given an average particle diameter of 80 nm and a filter solidity of 0.1[5], it is estimated that ~ 1 and 10 particle layers were present on the filters, respectively. Filters were stored at -16 °C immediately after collection until analysis.

Before sample treatment, each filter was cut into six identical slices. One of the six slices was set aside as a standard, while the other five were placed sequentially on a supporting mesh disc for F-TD/CIMS. In the thermal desorption process, the temperature of the N_2 flow above the filter was ramped at 10 °C min^{-1} (the typical working condition of FIGAERO-ToF-CIMS[5]) to maximum setpoints of 25, 50, 100, 150, and 200 °C; the 25 °C case corresponds to isothermal evaporation with dry N_2 at room temperature. After the temperature setpoint was achieved, the system was held at the setpoint for 50 min. Figure 1 diagrams the thermal desorption and extraction protocol and provides an example of the temporal profiles of thermal desorption for compounds at the same nominal m/z as pinic acid ($HF \cdot C_9H_{13}O_4^-$, m/z 205), a well-characterized α-pinene oxidation product, for filters with 300-min sample collection. Table S1 provides an overview of the treatment applied to each filter sample.

UPLC/(−)ESI-Q-TOF-MS

Following thermal desorption, each filter, along with the standard, was extracted in 1 mL ultra-pure water (18 MΩ, < 3 ppb TOC, Millipore Milli-Q) with a mini vortexer (VMR) for 1 h at room temperature. The extracts were then delivered to the ultra-performance liquid chromatography/negative electrospray ionization quadrupole time-of-flight mass spectrometer (UPLC/(−)ESI-Q-TOF-MS, hereafter UPLC/ESI-MS) for analysis of the remaining components on the filters.[28,29] Briefly, filter extracts were separated by a Waters ACQUITY UPLC I-Class system equipped with an ACQUITY BEH C_{18} column (1.7 μm, 2.1 mm × 50 mm) fitted with an ACQUITY BEH C_{18} VanGaurd pre-column (1.7 μm, 2.1 mm × 5 mm) at 30 °C. Samples were injected with a 10 μL volume, and the total flow rate through the

column was 0.3 mL min^{-1}. Eluate was ionized by ESI in negative ion (−) mode and sent to a Xevo G2-S Q-TOF-MS where ions are detected as $[M-H]^-$. The mass resolution ($m/\Delta m$) is 20,000-34,000 with a mass accuracy of <5 mDa. Molecular formulas ($C_xH_yO_z$) were assigned with errors of <7 ppm. Details of the gradient-elution method, instrument working conditions and acquisition parameters, calibration protocol, and data analysis can be found elsewhere.[28,29] Note that as a result of the guard column, the SOA molecular products elute at later retention times (+0.11-0.15 min) than previously reported.[28–30]

Direct Evaporation of Particles

The design of the filter holder provides the flexibility to quickly transition between different applications. For example, the hole for Probe 1 is suitable for a standard 1/4" critical orifice, which can be used for direct sampling of aerosols in the absence of the porous disc (Fig. S1b). In this setup, the temperature-ramped N_2 flow mixes with the aerosol flow and evaporates the condensed-phase compounds immediately before the IMR chamber. The temperature of the N_2 flow at the mixing point has been verified to have a linear relationship with the temperature of the heating tube, so only Probe 2 is necessary. The mixing and evaporating time is on the order of 0.1 s; thus, only a portion of the condensed organic matter evaporates before the particles exit the F-TD inlet (i.e., the compounds in the gas and particle phases have not reached equilibrium during this period[4]). The change of CIMS signal S thus follows Eq. (1):

$$S = (E(T) - D(T)) \times \tau + I \quad (1)$$

where $E(T)$ and $D(T)$ are the temperature-dependent particle evaporation and thermal decomposition rates, τ is the residence time in the heating region, and I is the initial CIMS signal without heating. This setup is used to evaluate the thermal stability of particle-phase compounds (e.g., ROOH). As higher temperature promotes faster evaporation from the particle phase ($E \propto T$), one would expect that the CIMS signal of a thermally stable

compound analyzed in this way should always increase as temperature increases (i.e., $E > D$ or $D = 0$). Accordingly, a decreasing signal as a function of increasing temperature will serve as an indication that a compound has undergone thermal decomposition at high temperature, since the decomposition rate must exceed the evaporation rate (i.e., $E < D$).

Data Analysis

The thermal desorption profile for a given compound deposited on a filter reflects its gas-phase concentration (mass volume^{-1}) determined by the evaporation flux (mass time^{-1}) and the carrier gas flow rate (volume time^{-1}) in CIMS. The integrated mass evaporated from the filter sample (N_{evap}) and the remaining mass on the filter (N_{remain}) are complementary:

$$N_{\text{tot}} - N_{\text{remain}} = N_{\text{evap}} = \int_0^t J(t')dt' = (\dot{T})^{-1} \int_{T_0}^{T_s} J(T')dT' + \int_{t(T_s)}^t J(t')dt' \qquad (2)$$

where $J(t')$ and $J(T')$ represent the evaporation flux (mass time^{-1}) as a function of time or temperature, $\dot{T}$ is the linear heating rate (°C s^{-1}), and T_0 and T_s are the initial temperature and setpoint, respectively. The first term on the right-hand-side (RHS) of Eq. (2) is the integral of flux during the temperature ramping period (i.e., the conventional thermogram), and the second term represents the integral of flux when temperature is held constant at the setpoint. Fig. 1 shows the temporal profile of the evaporation flux during ramping and holding periods.

The flux, $J(t')$ or $J(T')$, coming off the filter is proportional to the product of the sample vapor pressure (which increases as temperature increases) and the available surface area of the sample (which decreases with time).[31] Thus, the evaporation flux of a specific compound during thermal desorption exhibits a maximum value at a corresponding temperature, T_{max}. In addition to vapor pressure and available surface area, the thermal desorption profile of a compound also depends on the rate of reversible oligomerization, and the rate of thermal decomposition of oligomers.[5] The thermal desorption profile, therefore, is not a simple curve

that can be analytically represented. We fit the first term of the RHS of Eq. (2) to a Gaussian distribution using the simplified fitting procedure of Lopez-Hilfiker et al.[13], which shows good agreement ($R^2 > 0.9$). Note that the raw CIMS data have been corrected by the background signal (i.e., the signal of a blank filter subjected to the temperature ramp).

For desorption driven only by a temperature ramp, if the thermal desorption profile arises solely from authentic compounds and not desorption artifacts (e.g., decomposition), then the MFR of those compounds on the filter should be 50% at $T_{\max}$. The equation for this behavior has the form of a complementary error function: $f(T) = \mathrm{erfc}(\frac{T-T_{\mathrm{mid}}}{\sigma_r}) = 1 - N_{\mathrm{evap}}$, where T_{mid} corresponds to the temperature at which the MFR is 50%, and σ_r relates to the width of the desorption peak (an indicator of isomers, which could broaden the peak and thus increase σ_r). Note that although a sigmoidal curve is usually applied to fit the MFR of aerosol-phase components derived from thermodenuder measurement,[32] we choose the error function to be consistent with the Gaussian fitting of the thermogram.

Since the filters were held at the temperature setpoint for 50 min after the temperature ramp (the second term on the RHS of Eq. (2)), the MFR on the filter at the end of the thermal desorption will be lower than that derived by considering only the integral of the Gaussian distribution (the first term on the RHS of Eq. (2)). Thus, for the desorption profiles presented here, T_{mid} must be $< T_{\max}$ when the profile is only a result of the authentic compounds. If $T_{\mathrm{mid}} \geq T_{\max}$, the desorption profile could result from thermal decomposition, which can be further constrained with the UPLC/ESI-MS data. See Fig. S5 for clarification.

Owing to the inability of techniques that measure the evaporation flux during thermal desorption events to discriminate between signals due to authentic compounds vs. artifacts of thermal decomposition, it is not possible to calculate the MFR of individual compounds from thermal desorption profiles based on CIMS signals. As such, in this study the MFR is calculated from UPLC/ESI-MS data by taking the ratio of compound mass on the treated filters to that on the standard filter. As a result, the MFR reported in this study includes both the residual compound mass in the aerosol phase as well as that which may have been

adsorbed on the filter surface. This is in contrast to Schobesberger et al.[5], which distinguished the mass in the aerosol phase from that on the filter. This approach to calculating MFR also differs from that presented in D'Ambro et al.[17], which defines the signal fraction remaining (SFR) as the ratio of integrated thermograms prior to and following an isothermal evaporation period. The concept of SFR thus includes the contribution of the second peak in the thermogram, which is understood to be due to thermal decomposition of oligomers.

Results and Discussion

F-TD of α-pinene ozonolysis SOA yields two sets of complementary data: the evaporation flux monitored by CIMS and the residual filter components detected by UPLC/ESI-MS. The following discussion starts from the thermal desorption of SOA filter samples, proceeds to analysis of the remaining mass on the filter, and concludes with insights afforded from the combination of these two data sets. The evaporation of aerosol introduced directly into the F-TD/CIMS provides additional information on the thermal stability of aerosol-phase compounds.

Thermal Desorption of α-pinene Ozonolysis SOA

The room temperature (25 °C) thermal desorption scenario is analogous to isothermal evaporation. The decreasing desorption profile of compounds with a nominal m/z of 203, assumed to correspond almost exclusively to pinonic acid ($HF \cdot C_{10}H_{15}O_3^-$) upon isothermal evaporation is shown in Fig. S6 for filter samples collected for 30 and 300 min. Although the evaporation fluxes of the 30- and 300-min filter samples show similar trends, the absolute fluxes do not scale by a factor of 0.1 (the ratio of aerosol mass loading for the 30- and 300-min collections, assuming the evaporation flux from single particles do not interact). This suggests that the aerosol mass loading on the filter affects the evaporation rate. D'Ambro et al.[17] observed an initial rapid decrease in flux followed by slow decay during isothermal

evaporation of semi-volatile organic compounds from fresh α-pinene SOA. Such behavior could be a result of the slow diffusion of vapor molecules within multi-particle layers, a process that increases in importance at high aerosol mass loading.

Figure 2 shows the thermograms of compounds with the same nominal m/z as pinonic acid ($HF \cdot C_{10}H_{15}O_3^-$, m/z 203) and pinyl-diaterpenyl ester ($HF \cdot C_{17}H_{25}O_8^-$, m/z 377), two well-characterized α-pinene oxidation products,[30] for 30- and 300-min filter collection durations. Thermograms at four temperature setpoints (50, 100, 150, and 200 °C) are overlaid, illustrating that the thermal desorption behavior of compounds on a filter sample is independent of the temperature setpoint. A double-Gaussian function fits the raw thermogram data well ($R^2 > 0.9$). The first peak in the thermogram corresponds to the compound that is initially present in the SOA, while the second peak arises from the thermal decomposition of oligomers. From this fitting, the first peak in the thermogram can be compared and verified against the MFR on the filter, as explained in *Data Analysis*.

The compounds shown in Fig. 2 represent α-pinene-derived monomers (a and c) and dimers (b and d), respectively. For the monomers, a distinctive narrow peak (T_{max}) exists at $\sim$ 50 °C for both 30- and 300-min filter samples. This value exceeds that obtained from pure pinonic acid (<32 °C),[33] which can be explained by enhanced non-covalent H-bonding between pinonic acid and the SOA matrix as well as by the presence of isomeric/isobaric oxidation products.[5] Particle phase state could also affect the value of T_{max}, since α-pinene SOA can be semi-solid under the dry conditions[34] employed in this work (25 °C, <1% RH), which may retard the rate of evaporation. The second peak of the monomer thermogram is indicative of thermal decomposition of oligomers at high temperature. The shape of the second peak in Fig. 2a is the same as those observed by Lopez-Hilfiker et al.[33]. Note that the second peaks of Figs. 2a and 2c exhibit different behavior, with the 300-min filter sample having a higher peak temperature (100 vs. 130 °C). Fig. S7 shows thermograms for compounds with the same nominal m/z as pinic acid ($HF \cdot C_9H_{13}O_4^-$, m/z 205), norpinic acid ($HF \cdot C_8H_{11}O_4^-$, m/z 191), HO-pinonic acid ($HF \cdot C_{10}H_{15}O_4^-$, m/z 219), and diaterpenylic

acid ($HF \cdot C_8H_{13}O_5^-$, m/z 209) for 30- and 300-min filter samples. No apparent dependence of the T_{max} values of all monomers in 30- and 300-min filter samples (Table S2) on filter aerosol mass loading was observed. This is consistent with the work of Huang et al.[18], which reported a trend of increasing T_{max} as a function of aerosol mass loading that plateaued when aerosol mass loading increased to $> \sim 1$ μg cm^{-2}, the regime in which the current filter samples lie (≥ 1 μg cm^{-2}). Moreover, for all monomers, the second peak occurs at a higher temperature for the 300-min filter samples.

For the dimer shown in Figs. 2b and 2d, at lower aerosol mass loading, the thermogram exhibits a wide single peak at ~ 140 °C, whereas for higher mass loading, a bi-modal thermogram is observed. Similarly to the monomers, the first peak at 95 °C in Fig. 2d is assigned to evaporation of authentic dimer (with the same nominal m/z as pinyl-diaterpenyl ester), whereas the second peak at 165 °C is attributed to thermal decompositon of oligomers with m/z greater than the dimers observed. The broad single peak in Fig. 2b is thought to be due solely to thermal decompsotion and, like the monomers, occurs at a lower temperature (140 °C) in the 30-min filter samples. We hypothesize that the difference in temperature of the second peak between the 30- and 300-min samples for both monomers and dimers is a result of larger absolute amounts of oligomers being deposited on the filter at higher aerosol mass loadings and undergoing decomposition at higher temperature.

Remaining Fraction on Filters

Figure 3 shows the UPLC base peak ion (BPI) chromatograms of six filter samples: a fresh filter that is used as a reference, and five filters that have undergone thermal desorption in the F-TD system. The molecular formulas and proposed structures of dominant compounds are marked. The chromatograms of 30- and 300-min filter samples before any treatment have similar product distributions, indicating that the mass fractions of these species are independent of collection time. However, given the dependence of ESI efficiency on molecular structure, namely that the ESI efficiences of dimers are at least an order of magnitude higher

than those of monomers, the peak areas of the detected compounds are not proportional to their relative abundances on the filter.[23] The chromatogram can be roughly divided into two regions based on retention time (t_R) and thus molecular size: most of the peaks at $t_R <$ 5.4 min with cold colors (blue and green) correspond to monomer acids, while those eluted later with warm colors (orange and red) are dimer acids. Whereas most of the monomers on the filter have fully evaporated at higher temperature setpoints ($\geq$ 100 °C), the persistence of dimer peaks (e.g., pinyl-diaterpenyl ester and pinonyl-pinyl ester) up to temperature setpoints of 150 °C suggests that SOA monomers and dimers evaporate at different rates upon heating. For some of the dimers, over 50% of the collected filter mass remains for the 300-min filter sample at 150 °C. Furthermore, the appreciable MFR values derived from UPLC/ESI-MS demonstrate that the sharp decrease in normalized signal to <0.05 during the 50-min desorption at the temperature setpoint (Fig. 2) is not a result of the particle-phase compounds having been fully desorbed, but rather is likely due to the particle morphology having been modified upon heating, thereby limiting further evaporation.

For the system studied here, 53 main products were identified from the UPLC/ESI-MS data (Table S3). Fig. 4 shows the MFR (i.e., chromatographic peak area normalized by that of the fresh filter samples) of eight prominent monomeric and dimeric α-pinene oxidation products, previously characterized by LC/ESI-MS,[35,36] as a function of temperature setpoint for the 30- and 300-min filter samples. Interestingly, for both 30- and 300-min filter samples, isothermal evaporation at room temperature resulted in a MFR for dimers statistically greater than 1, while the MFR of monomers decreased in accord with their volatility. This behavior points to an additional source of dimers on the filter. Since isothermal evaporation is carried out with pure N_2 in a dark environment (i.e., oxidant- and photolysis-free), the likely source of dimers on the filter appears to be reversible oligomerization,[5] forming dimers either via decomposition of oligomers or accretion of monomers. Owing to their lower volatility, dimers produced through either oligomer decomposition or monomer accretion will accumulate on the filter, while monomers formed from oligomer decomposition will evaporate

based on their volatility.[5]

T_{mid} (dashed horizontal line in Fig. 4a and b) is smaller than T_{max} (e.g., Fig. 2) for all of the monomers in 30-min filter samples. This behavior verifies that the first peak in the thermogram arises from direct evaporation of monomers initially present in the aerosol. Generally, T_{mid} is higher for 300-min filter samples than those for 30-min filter samples, confirming the effect of aerosol mass loading on the compound evaporation rates.[18] Table S2 summarizes T_{max} and T_{mid} for six compounds in this study.

$C_8H_{12}O_4$ isomers assigned to terpenylic and norpinic acid exhibit virtually the same MFR decay profile for the 300-min sample (Fig. 4b) The thermogram for compounds with the same nominal m/z as terpenylic and norpinic acid ($HF \cdot C_8H_{11}O_4^-$, m/z 191) also has a narrow first peak (Fig. S7), suggesting that monomer isomers do not cover a wide range of saturation vapor pressure. The narrow thermogram and similar MFR profiles indicate that despite the notable structural dissimilarities between terpenylic and norpinic acids, the thermal behavior of the isomers is similar. However, additional measurements are needed to confirm the generality of this observation. The large σ_r of the two dimers in the 30-min filter sample (illustrated in Fig. 4a by the shallow slope of the fit) is consistent with the observed broad Gaussian distribution in their thermograms (Fig. 2), further suggesting that thermal decomposition of oligomers could be an important source of dimers upon heating.

At large aerosol mass loading, a high fraction of dimers remains on the filter at high temperatures, with 50 min at 200 °C required for full evaporation. Below 200 °C, the dimer MFR is higher for all temperatures at higher mass loading. This has been suggested to be the result of an artifact: multi-particle layers on the filter due to long collection time limit the vapor diffusion between layers.[18,37] The effect of high mass loading on the volatility of filter samples is also exemplified by the compound $C_8H_{14}O_5$ (the same molecular formula as diaterpenylic acid), which has a T_{mid} of $\sim$ 100 °C for the 300 °C sample, well exceeding the T_{mid} of $\sim$ 40 °C for the 30-min sample and T_{max} of $\sim$ 50 °C in its thermogram (Fig. S7). Since the width of the thermogram is large, the profile of $C_8H_{14}O_5$ could be a result of

oligomer dissociation at high aerosol mass loading.

Thermal Stability of SOA Molecular Products

Thermal decomposition of monomers, dimers, and oligomers, particularly those with labile functionalities [e.g., organic (hydro)peroxides], occurs in thermal-induced desorption of SOA.[13,20,38,39]

Monomers

We first use the direct evaporation of aerosol-phase components to evaluate the thermal stability of compounds expected to contain ROOH moities.[40,41] The CF_3O^--CIMS has been shown to have high sensitivity to ROOH via reagent ion clustering ($ROOH \cdot CF_3O^-$).[24,25] Figure S8 shows the thermograms of two classes of α-pinene ozonolysis products with distinct desorption behaviors (i.e., increasing vs. decreasing signal intensity with increasing desorption temperature). The signal of the nominal m/z assigned to pinonic acid, a relatively volatile species, increases by $\sim$ 25% at 200 vs. 25 °C, while the signals attributed to pinic acid and OH-pinonic acid at 200 °C are a factor of 2-3 higher than those at 25 °C. In contrast, the signals previously assigned to ROOH species[30,41] decrease at 200 °C to 30 - 50% of their intensities at 25 °C. Generally, higher temperature prompts faster evaporation flux from particles; thus the signals should monotonically increase as temperature increases. Since the ionization efficiency is not a function of temperature (i.e., the kinetics in the IMR are already in the collision-limited regime[42]), the increasing signal upon heating is due to accelerated evaporation ($E > D$) or transformation from other species through chemical reactions (e.g., thermal decomposition of oligomers), whereas the decreasing trend is a result of thermal instability at high temperature ($E < D$). For example, Pagonis and Ziemann[43] reported that particle-phase chemistry of hydroperoxycarbonls can eliminate the $-$OOH group. Note that gas-phase species, including O_3, were not removed before introducing aerosols to the heating region, which could lead to artifacts via oxidation at high temperature.[44] We also

cannot exclude the possibility of ROOH decomposition on the metal surface at high temperature as a possible artifact, since the inside surface of IMR was not coated with an inert material (e.g., Teflon). Particle-phase peroxides are known to be labile[45], making detection challenging. The thermal instability of compounds expected to contain ROOH demonstrated here through direct evaporation of α-pinene SOA suggests that F-TD may not be the best method to study condensed-phase peroxides.[29]

Dimers

Since α-pinene-derived oligomers (carbon number > 20) are not detected by either F-TD/CIMS or UPLC/ESI-MS, we evaluated two possible mechanistic hypotheses concerning the fate of dimers to explain the observed modes in the monomer and dimer thermograms: (1) thermal decomposition of dimers at high temperature; (2) heat-induced accretion of monomers.

F-TD was performed on a synthesized pinene-derived dimer ester standard (Fig. 5a; see Kenseth et al.[23] for synthesis and characterization details) that was dissolved in ethanol and deposited on a filter by a microsyringe. CIMS signals corresponding to the monomeric decomposition products (i.e., pinonic acid and pinolic acid) of the dimer via cleavage of the ester bond were not observed under standard thermal desorption conditions. This conclusion agrees with that of Claflin and Ziemann[39] that esters are stable at high temperature.

The possible formation of dimers from monomers upon heating was also explored, since, as indicated by the higher MFR values at higher mass loading (see Section **Remaining Fractions on Filters**), the morphology and/or composition of the particles changes upon heating-induced evaporation and may increase the probability of condensed-phase reactions. To carry out this test, equimolar (~ 35 μmol) masses of enantiopure *cis*-pinic acid (see Kenseth et al.[23] for synthesis and characterization details) and enantiopure β-pinene diol (synthesis and characterization details available on request) were ground and deposited on a filter, instead of dissolving the compounds in ethanol and depositing the solution. Since

the thermograms of observed dimers in α-pinene SOA exhibit $T_{\max}$ of $\sim$ 100 °C (Fig. 2), the F-TD was maintained at 100 °C until complete desorption of the sample was achieved. Instead of sending the resulting hot and highly concentrated vapors to the CIMS, a Teflon filter was placed $\sim$ 0.5 m downstream to capture nucleated particles formed due to the steep temperature gradient; the filter was then extracted and delivered to the UPLC/ESI-MS. The UPLC BPI chromatogram is shown in Fig. 5b. In contrast to the result of Zhao et al.[21] that mixed organic acids displayed no oligomer formation on heating, four distinct dimer peaks with the formula $C_{19}H_{30}O_5$ [i.e., the formal condensation product of *cis*-pinic acid ($C_9H_{14}O_4$) and β-pinene diol ($C_{10}H_{18}O_2$)] are observed. The absence of observable dimer formation in a control experiment in which an equimolar ($\sim$ 1.0 mM) aqueous solution of the two monomers was directly subjected to UPLC/ESI-MS demonstrates that these monomers undergo thermally induced condensation reactions (e.g., esterification) during F-TD analysis rather than on the filter or in solution at 25 °C. This experiment indicates that at high temperature, if monomers remain, dimer formation via thermal accretion chemistry is possible. This situation is most likely to occur under high aerosol mass loading and (semi-)solid particle phase state, or when temperature increases rapidly (e.g., a step increase of the temperature in a thermodenuder), where the limitation of monomer evaporation increases the likelihood of accretion reactions. Note that particle-phase reaction could also occur over time in the absence of oxidants even at room temperature.[46,47]

Atmospheric Implications

Filter-based thermal desorption is widely used to analyze SOA molecular constituents. We show here that aerosol mass loadings higher than typically collected for filter-based thermal desorption can lead to significantly different characteristics of the thermal desorption profile, likely an artifact arising from diffusion limitations of vapor molecules between the multiple particle layers deposited on the filter. This situation can be viewed as analogous to that in which a (semi-)solid particle phase state limits vapor diffusion within particles. The

condensation of acid and alcohol monomers to form dimers (likely ester dimers) upon fast heating provides direct evidence that unexpected, thermally driven particle-phase chemistry could bias the analysis of the thermogram.

Simultaneous examination of both gas- and particle-phase components provides direct evidence that the second peak at higher temperature in the thermograms of monomers is a result of thermal decomposition of oligomers. Though it is not possible to resolve those oligomers that contribute to the second peak in the thermogram with the current technique, we have demonstrated that the first peak of the thermogram arises from evaporation of pure compounds through combination with UPLC/ESI-MS, which resolves the remaining compounds on the filter. The UPLC/ESI-MS is able to isolate isomers, further verifying that the multi-mode thermogram of a monomer is not a result of isomers with distinct volatility but arises from the thermal decomposition of oligomers.

With the direct evaporation of aerosol samples, we demonstrate that particle-phase compounds assigned to ROOH, a highly labile species, undergo decomposition as temperature increases; however, the decomposition trends as a function of temperature are compound-dependent. In contrast, a synthesized pinene-derived dimer ester, a representative surrogate of dimers present in α-pinene ozonolysis SOA, exhibits thermal stability at high temperature. Thus, thermal desorption works well for thermally stable condensed-phase compounds, but is not an appropriate method to quantitatively resolve labile particle-phase species.

Thermally-induced evaporation of SOA separates the condensed-phase components based on their volatility, a process for which heat-accelerated condensed-phase reactions (e.g., oligomerization and decomposition) are highly likely. Interpretation of evaporation flux of possible isomers or dissociation of oligomers can be constrained from the remaining components on the filter. Using the dry α-pinene ozonolysis nucleation system, we demonstrate that the complementary F-TD/CIMS + UPLC/ESI-MS method of detecting SOA components at the molecular level provides important insights into SOA formation.

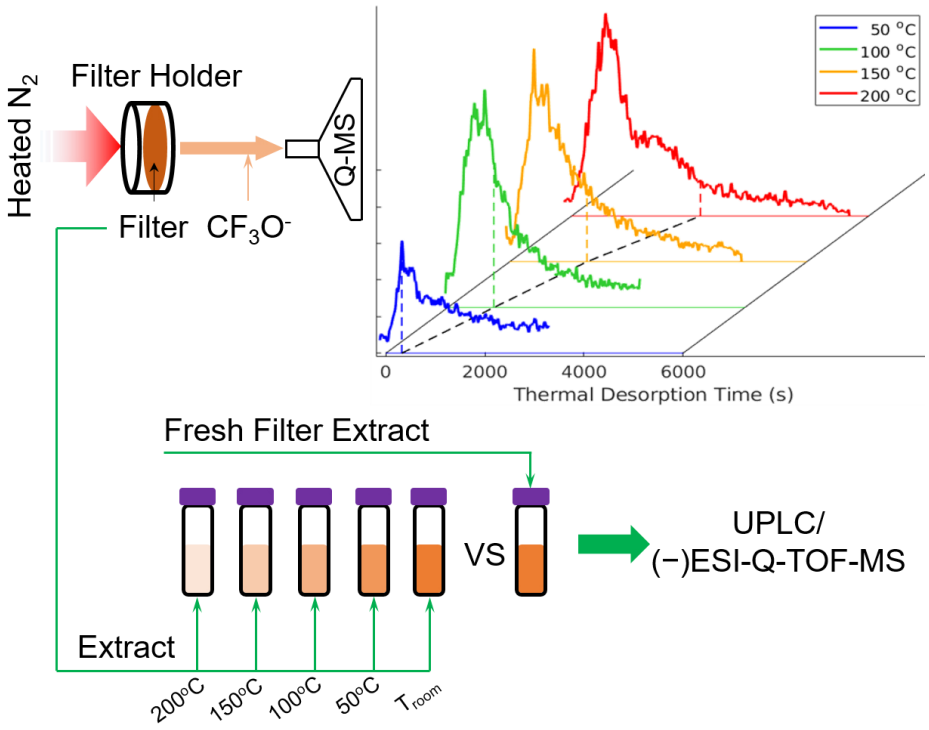

Figure 1: Filter-based thermal desorption experimental protocol. Filter samples are first thermally desorbed via the F-TD inlet system for CF_3O^--CIMS. Filters are then extracted with H_2O at room temperature into vials that are subsequently delivered to UPLC/(−)ESI-Q-TOF-MS. Heated N_2 is ramped to different temperatures at 10 °C min^{-1} and held for 50 min to allow sufficient evaporation. Temporal profiles of thermal desorption of compound(s) at the same nominal m/z as pinic acid ($HF \cdot C_9H_{13}O_4^-$, m/z 205) are shown as an example. Curve colors correspond to thermal desorption with temperature setpoints of 50 (blue), 100 (green), 150 (orange), and 200 (red) °C. Dashed vertical lines indicate the time at which the temperature setpoint has been reached. The black dashed line tracks the temperature setpoints for different desorptions.

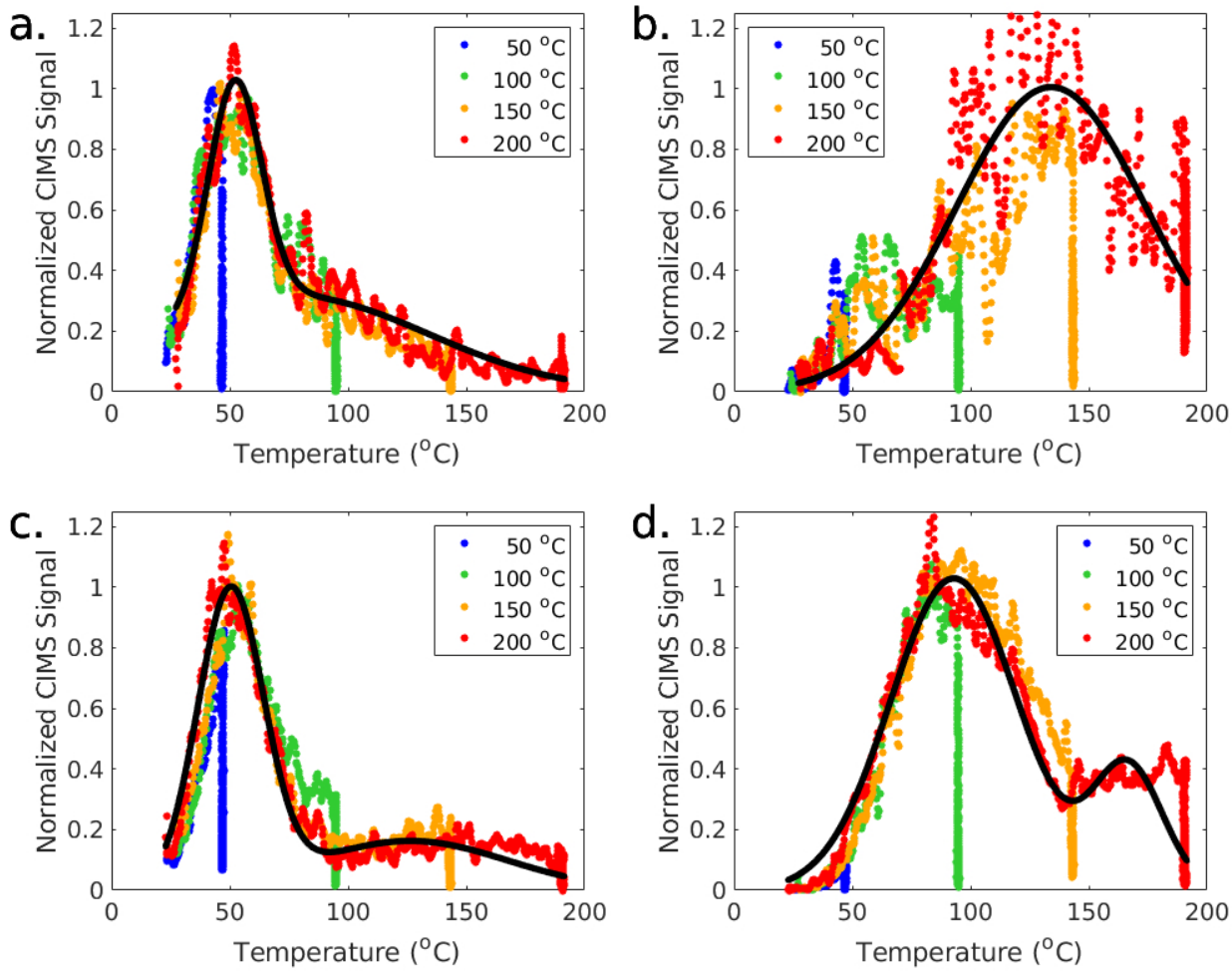

Figure 2: Thermograms of compounds with the same nominal m/z as pinonic acid ($HF \cdot C_{10}H_{15}O_3^-$, m/z 203, Panel a and c for 30- and 300-min filter collection, respectively) and pinyl-diaterpenyl ester ($HF \cdot C_{17}H_{25}O_8^-$, m/z 377, Panel b and d for 30- and 300-min filter collection, respectively). Black lines are double-Gaussian fitting curves applied to the 200 °C thermogram. The four data sets (blue, green, orange, and red) correspond to the different temperature setpoints (50, 100, 150, and 200 °C) to which the filters were ramped and then held for 50 min.

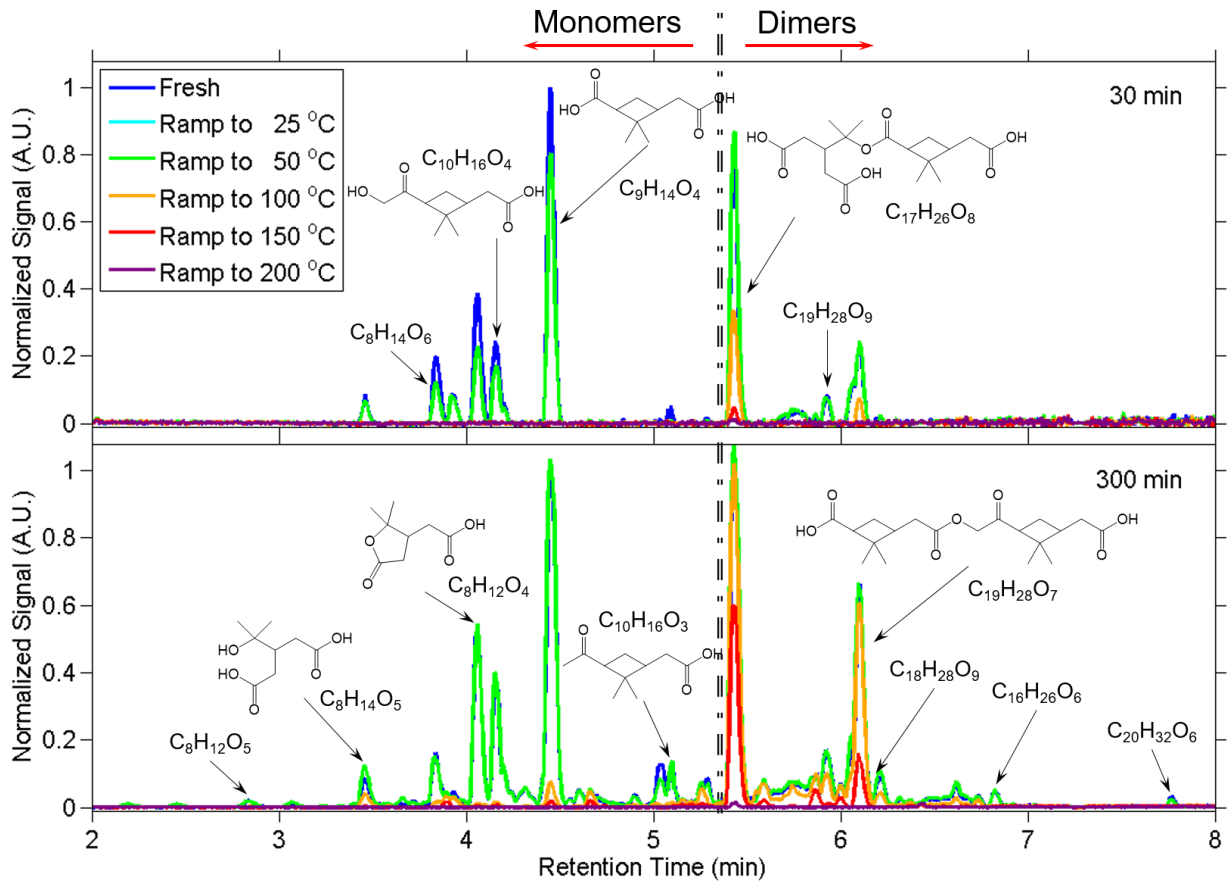

Figure 3: UPLC/(−)ESI-Q-TOF-MS BPI chromatograms of SOA formed from α-pinene ozonolysis in the CPOT, collected on Teflon filters for 30 (upper) and 300 min (lower). Molecular formulas and/or proposed structures for the dominant peaks are shown. Chromatogram colors correspond to the temperature setpoints at which the filters were thermally desorbed by the F-TD system prior to extraction. The chromatogram is roughly divided into monomer and dimer regimes based on identified molecular formulas and retention time.

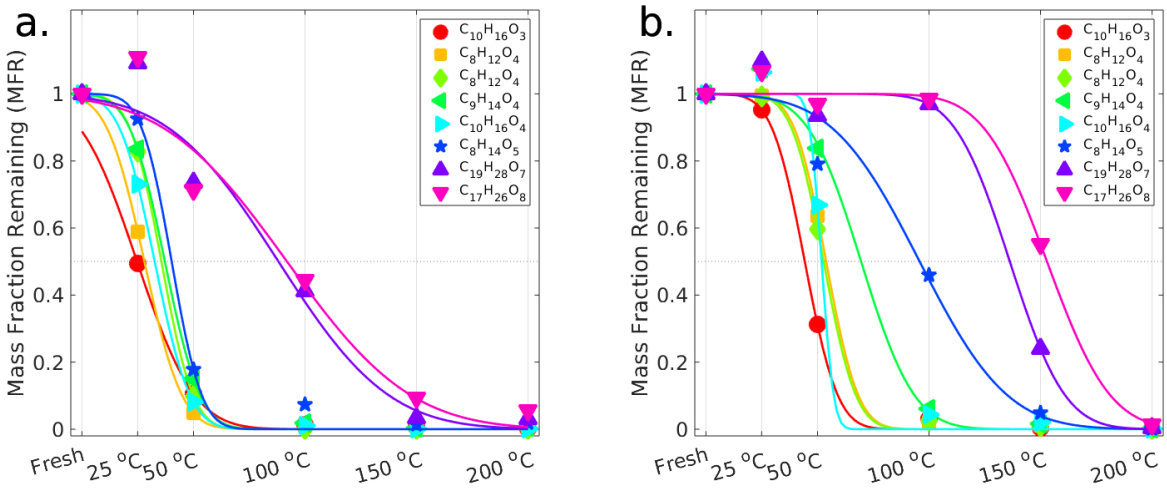

Figure 4: Mass fraction remaining (MFR) of eight compounds identified in SOA from α-pinene ozonolysis and assigned to well-characterized oxidation products (pinonic acid $C_{10}H_{16}O_3$, terpenylic (■) and norpinic (♦) acids $C_8H_{12}O_4$, pinic acid $C_9H_{14}O_4$, HO-pinonic acid $C_{10}H_{16}O_4$, diaterpenylic acid $C_8H_{14}O_5$, pinonyl-pinyl ester $C_{19}H_{28}O_7$, and pinyl-diaterpenyl ester $C_{17}H_{26}O_8$) as a function of the temperature setpoints at which filters were thermally desorbed by the F-TD system before extraction for (a) 30- and (b) 300-min filter collection. Data points are fitted by the complementary error function $f(T) = \mathrm{erfc}(\frac{T-T_{\mathrm{mid}}}{\sigma_r})$ (see *Data Analysis* for details).

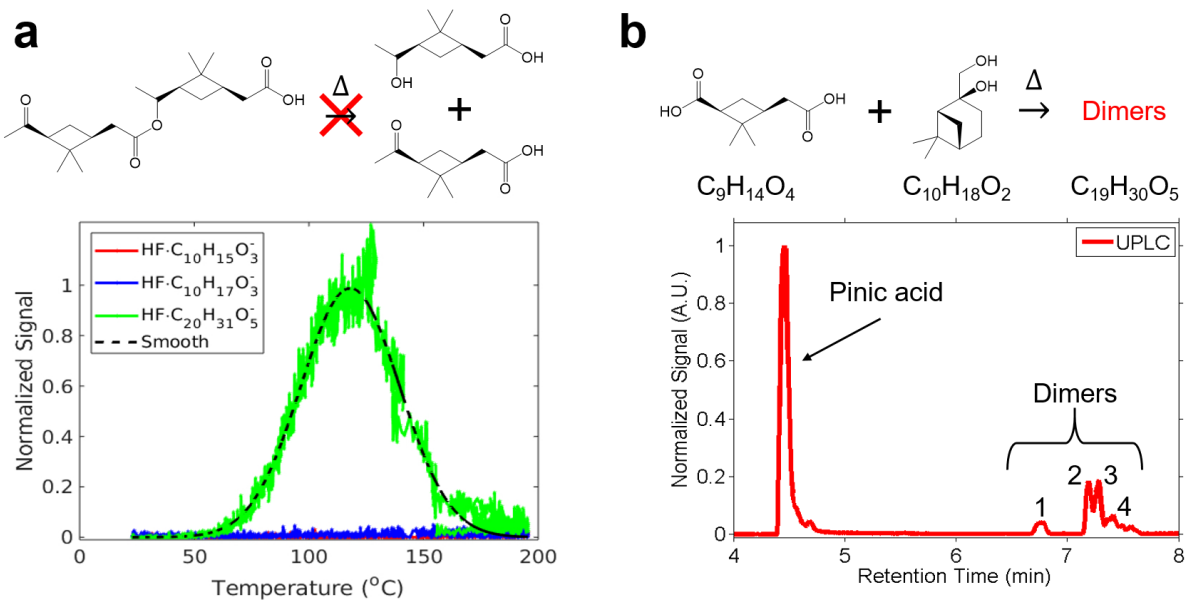

Figure 5: a: Thermogram of a synthesized pinene-derived ester ($HF \cdot C_{20}H_{31}O_5^-$, m/z 371). The absence of signals at the same nominal m/z as monomeric decomposition products, pinonic acid ($HF \cdot C_{10}H_{15}O_3-$,$m/z$ 203) or pinolic acid ($HF \cdot C_{10}H_{17}O_3^-$, m/z 205) during the temperature ramp suggests that the ester is stable at high temperature, consistent with the conclusion by Claflin and Ziemann[39]. b: UPLC/(−)ESI-Q-TOF-MS BPI chromatogram of a mixture of enantiopure *cis*-pinic acid ($C_9H_{14}O_4$) and β-pinene diol ($C_{10}H_{18}O_2$) after heating at 100 °C in the F-TD inlet. The appearance of four distinct dimer peaks ($C_{19}H_{30}O_5$) demonstrates that heating has induced condensation of *cis*-pinic acid and β-pinene diol.

Acknowledgement

We appreciate insightful discussions with John D. Crounse and Lu Xu. We acknowledge generous support from Dwight and Christine Landis.

Supporting Information Available

The supplementary material contains: I. Filter-Based Thermal Desorption System; II. Performance of F-TD; III. Sample Generation; IV. Data Analysis; V. Isothermal Evaporation; VI. Thermograms; VII. Identified Main Compounds from UPLC/ESI-MS; VIII. Decomposition of Hydroperoxides.

References

(1) George, I. J.; Abbatt, J. P. D. Heterogeneous oxidation of atmospheric aerosol particles by gas-phase radicals. *Nat. Chem.* **2010**, *2*, 713.

(2) Reid, J. P.; Bertram, A. K.; Topping, D. O.; Laskin, A.; Martin, S. T.; Petters, M. D.; Pope, F. D.; Rovelli, G. The viscosity of atmospherically relevant organic particles. *Nat. Commun.* **2018**, *9*, 956.

(3) Chow, J. C.; Yu, J. Z.; Watson, J. G.; Ho, S. S. H.; Bohannan, T. L.; Hays, M. D.; Fung, K. K. The application of thermal methods for determining chemical composition of carbonaceous aerosols: A review. *J. Environ. Sci. Health A* **2007**, *42*, 1521–1541.

(4) Cappa, C. D. A model of aerosol evaporation kinetics in a thermodenuder. *Atmos. Meas. Tech.* **2010**, *3*, 579–592.

(5) Schobesberger, S.; D'Ambro, E. L.; Lopez-Hilfiker, F. D.; Mohr, C.; Thornton, J. A. A model framework to retrieve thermodynamic and kinetic properties of organic aerosol from composition-resolved thermal desorption measurements. *Atmos. Chem. Phys.* **2018**, *18*, 14757–14785.

(6) Hearn, J. D.; Smith, G. D. A chemical ionization mass spectrometry method for the online analysis of organic aerosols. *Anal. Chem.* **2004**, *76*, 2820–2826.

(7) Smith, J. N.; Moore, K. F.; McMurry, P. H.; Eisele, F. L. Atmospheric measurements of sub-20 nm diameter particle chemical composition by thermal desorption chemical ionization mass spectrometry. *Aerosol Sci. Technol.* **2004**, *38*, 100–110.

(8) DeCarlo, P. F.; Kimmel, J. R.; Trimborn, A.; Northway, M. J.; Jayne, J. T.; Aiken, A. C.; Gonin, M.; Fuhrer, K.; Horvath, T.; Docherty, K. S.; Worsnop, D. R.; Jimenez, J. L. Field-deployable, high-resolution, time-of-flight aerosol mass spectrometer. *Anal. Chem.* **2006**, *78*, 8281–8289.

(9) Huffman, J. A.; Ziemann, P. J.; Jayne, J. T.; Worsnop, D. R.; Jimenez, J. L. Development and characterization of a fast-stepping/scanning thermodenuder for chemically-resolved aerosol volatility measurements. *Aerosol Sci. Technol.* **2008**, *42*, 395–407.

(10) Cappa, C. D.; Wilson, K. R. Evolution of organic aerosol mass spectra upon heating: implications for OA phase and partitioning behavior. *Atmos. Chem. Phys.* **2011**, *11*, 1895–1911.

(11) Tobias, H. J.; Ziemann, P. J. Compound identification in organic aerosols using temperature-programmed thermal desorption particle beam mass spectrometry. *Anal. Chem.* **1999**, *71*, 3428–3435.

(12) Yatavelli, R. L. N.; Thornton, J. A. Particulate organic matter detection using a micro-orifice volatilization impactor coupled to a chemical ionization mass spectrometer (MOVI-CIMS). *Aerosol Sci. Technol.* **2010**, *44*, 61–74.

(13) Lopez-Hilfiker, F. D.; Mohr, C.; Ehn, M.; Rubach, F.; Kleist, E.; Wildt, J.; Mentel, T. F.; Lutz, A.; Hallquist, M.; Worsnop, D.; Thornton, J. A. A novel method for online analysis of gas and particle composition: description and evaluation of a filter inlet for gases and aerosols (FIGAERO). *Atmos. Meas. Tech.* **2014**, *7*, 983–1001.

(14) Williams, B. J.; Goldstein, A. H.; Kreisberg, N. M.; Hering, S. V. In situ measurements of gas/particle-phase transitions for atmospheric semivolatile organic compounds. *Proc. Natl. Acad. Sci. U.S.A.* **2010**, *107*, 6676–6681.

(15) Isaacman, G.; Kreisberg, N. M.; Yee, L. D.; Worton, D. R.; Chan, A. W. H.; Moss, J. A.; Hering, S. V.; Goldstein, A. H. Online derivatization for hourly measurements of gas- and particle-phase semi-volatile oxygenated organic compounds by thermal desorption aerosol gas chromatography (SV-TAG). *Atmos. Meas. Tech.* **2014**, *7*, 4417–4429.

(16) Yatavelli, R. L. N.; Stark, H.; Thompson, S. L.; Kimmel, J. R.; Cubison, M. J.; Day, D. A.; Campuzano-Jost, P.; Palm, B. B.; Hodzic, A.; Thornton, J. A.; Jayne, J. T.;

Worsnop, D. R.; Jimenez, J. L. Semicontinuous measurements of gas-particle partitioning of organic acids in a ponderosa pine forest using a MOVI-HRToF-CIMS. *Atmos. Chem. Phys.* **2014**, *14*, 1527–1546.

(17) D'Ambro, E. L.; Schobesberger, S.; Zaveri, R. A.; Shilling, J. E.; Lee, B. H.; Lopez-Hilfiker, F. D.; Mohr, C.; Thornton, J. A. Isothermal evaporation of α-pinene ozonolysis SOA: volatility, phase state, and oligomeric composition. *ACS Earth Space Chem.* **2018**, *2*, 1058–1067.

(18) Huang, W.; Saathoff, H.; Pajunoja, A.; Shen, X.; Naumann, K.-H.; Wagner, R.; Virtanen, A.; Leisner, T.; Mohr, C. α-Pinene secondary organic aerosol at low temperature: chemical composition and implications for particle viscosity. *Atmos. Chem. Phys.* **2018**, *18*, 2883–2898.

(19) Steiner, T. The hydrogen bond in the solid state. *Angew. Chem. Int. Ed.* **2002**, *41*, 48–76.

(20) Stark, H.; Yatavelli, R. L. N.; Thompson, S. L.; Kang, H.; Krechmer, J. E.; Kimmel, J. R.; Palm, B. B.; Hu, W.; Hayes, P. L.; Day, D. A.; Campuzano-Jost, P.; Canagaratna, M. R.; Jayne, J. T.; Worsnop, D. R.; Jimenez, J. L. Impact of thermal decomposition on thermal desorption instruments: advantage of thermogram analysis for quantifying volatility distributions of organic species. *Environ. Sci. Technol.* **2017**, *51*, 8491–8500.

(21) Zhao, Z.; Yang, X.; Lee, J.; Tolentino, R.; Mayorga, R.; Zhang, W.; Zhang, H. Diverse Reactions in Highly Functionalized Organic Aerosols during Thermal Desorption. *ACS Earth Space Chem.* **2020**, *4*, 283–296.

(22) Willoughby, A. S.; Wozniak, A. S.; Hatcher, P. G. A molecular-level approach for characterizing water-insoluble components of ambient organic aerosol particulates using ultrahigh-resolution mass spectrometry. *Atmos. Chem. Phys.* **2014**, *14*, 10299–10314.

(23) Kenseth, C. M.; Hafeman, N. J.; Huang, Y.; Dalleska, N. F.; Stoltz, B. M.; Seinfeld, J. H. Synthesis of carboxylic acid and dimer ester surrogates to constrain the abundance and distribution of molecular products in α-pinene and β-pinene secondary organic aerosol. *Environ. Sci. Technol.* submitted.

(24) Crounse, J. D.; McKinney, K. A.; Kwan, A. J.; Wennberg, P. O. Measurement of gas-phase hydroperoxides by chemical ionization mass spectrometry. *Anal. Chem.* **2006**, *78*, 6726–6732.

(25) St. Clair, J. M.; McCabe, D. C.; Crounse, J. D.; Steiner, U.; Wennberg, P. O. Chemical ionization tandem mass spectrometer for the in situ measurement of methyl hydrogen peroxide. *Rev. Sci. Instrum.* **2010**, *81*, 094102.

(26) Paulot, F.; Crounse, J. D.; Kjaergaard, H. G.; Kürten, A.; Clair, J. M. S.; Seinfeld, J. H.; Wennberg, P. O. Unexpected epoxide formation in the gas-phase photooxidation of isoprene. *Science* **2009**, *325*, 730–733.

(27) Huang, Y.; Coggon, M. M.; Zhao, R.; Lignell, H.; Bauer, M. U.; Flagan, R. C.; Seinfeld, J. H. The Caltech photooxidation flow tube reactor: design, fluid dynamics and characterization. *Atmos. Meas. Tech.* **2017**, *10*, 839–867.

(28) Kenseth, C. M.; Huang, Y.; Zhao, R.; Dalleska, N. F.; Hethcox, J. C.; Stoltz, B. M.; Seinfeld, J. H. Synergistic O_3 + OH oxidation pathway to extremely low-volatility dimers revealed in β-pinene secondary organic aerosol. *Proc. Natl. Acad. Sci. U.S.A.* **2018**, *115*, 8301–8306.

(29) Zhao, R.; Kenseth, C. M.; Huang, Y.; Dalleska, N. F.; Seinfeld, J. H. Iodometry-assisted liquid chromatography electrospray ionization mass spectrometry for analysis of organic peroxides: an application to atmospheric secondary organic aerosol. *Environ. Sci. Technol.* **2018**, *52*, 2108–2117.

(30) Zhang, X.; McVay, R. C.; Huang, D. D.; Dalleska, N. F.; Aumont, B.; Flagan, R. C.; Seinfeld, J. H. Formation and evolution of molecular products in α-pinene secondary organic aerosol. *Proc. Natl. Acad. Sci. U.S.A.* **2015**, *112*, 14168–14173.

(31) Cappa, C. D.; Lovejoy, E. R.; Ravishankara, A. R. Determination of evaporation rates and vapor pressures of very low volatility compounds: a study of the C_4-C_{10} and C_{12} dicarboxylic acids. *J. Phys. Chem. A* **2007**, *111*, 3099–3109.

(32) Emanuelsson, E. U.; Watne, Å. K.; Lutz, A.; Ljungström, E.; Hallquist, M. Influence of humidity, temperature, and radicals on the formation and thermal properties of secondary organic aerosol (SOA) from ozonolysis of β-pinene. *J. Phys. Chem. A* **2013**, *117*, 10346–10358.

(33) Lopez-Hilfiker, F. D.; Mohr, C.; Ehn, M.; Rubach, F.; Kleist, E.; Wildt, J.; Mentel, T. F.; Carrasquillo, A. J.; Daumit, K. E.; Hunter, J. F.; Kroll, J. H.; Worsnop, D. R.; Thornton, J. A. Phase partitioning and volatility of secondary organic aerosol components formed from α-pinene ozonolysis and OH oxidation: the importance of accretion products and other low volatility compounds. *Atmos. Chem. Phys.* **2015**, *15*, 7765–7776.

(34) Liu, P.; Li, Y. J.; Wang, Y.; Gilles, M. K.; Zaveri, R. A.; Bertram, A. K.; Martin, S. T. Lability of secondary organic particulate matter. *Proc. Natl. Acad. Sci. U.S.A.* **2016**, *113*, 12643–12648.

(35) Yasmeen, F.; Vermeylen, R.; Szmigielski, R.; Iinuma, Y.; Böge, O.; Herrmann, H.; Maenhaut, W.; Claeys, M. Terpenylic acid and related compounds: precursors for dimers in secondary organic aerosol from the ozonolysis of α- and β-pinene. *Atmos. Chem. Phys.* **2010**, *10*, 9383–9392.

(36) Yasmeen, F.; Vermeylen, R.; Maurin, N.; Perraudin, E.; Doussin, J.-F.; Claeys, M. Characterisation of tracers for aging of α-pinene secondary organic aerosol using liq-

uid chromatography/negative ion electrospray ionisation mass spectrometry. *Environ. Chem.* **2012**, *9*, 236–246.

(37) Kolesar, K. R.; Chen, C.; Johnson, D.; Cappa, C. D. The influences of mass loading and rapid dilution of secondary organic aerosol on particle volatility. *Atmos. Chem. Phys.* **2015**, *15*, 9327–9343.

(38) Hall IV, W. A.; Johnston, M. V. The thermal-stability of oligomers in alpha-pinene secondary organic aerosol. *Aerosol Sci. Technol.* **2012**, *46*, 983–989.

(39) Claflin, M. S.; Ziemann, P. J. Thermal desorption behavior of hemiacetal, acetal, ether, and ester oligomers. *Aerosol Sci. Technol.* **2019**, *53*, 473–484.

(40) Docherty, K. S.; Wu, W.; Lim, Y. B.; Ziemann, P. J. Contributions of organic peroxides to secondary aerosol formed from reactions of monoterpenes with O_3. *Environ. Sci. Technol.* **2005**, *39*, 4049–4059.

(41) Eddingsaas, N. C.; Loza, C. L.; Yee, L. D.; Seinfeld, J. H.; Wennberg, P. O. α-pinene photooxidation under controlled chemical conditions - Part 1: Gas-phase composition in low- and high-NO_x environments. *Atmos. Chem. Phys.* **2012**, *12*, 6489–6504.

(42) Lopez-Hilfiker, F. D.; Iyer, S.; Mohr, C.; Lee, B. H.; D'Ambro, E. L.; Kurtén, T.; Thornton, J. A. Constraining the sensitivity of iodide adduct chemical ionization mass spectrometry to multifunctional organic molecules using the collision limit and thermodynamic stability of iodide ion adducts. *Atmos. Meas. Tech.* **2016**, *9*, 1505–1512.

(43) Pagonis, D.; Ziemann, P. J. Chemistry of hydroperoxycarbonyls in secondary organic aerosol. *Aerosol Sci. Technol.* **2018**, *52*, 1178–1193.

(44) Batakliev, T.; Georgiev, V.; Anachkov, M.; Rakovsky, S.; Zaikov, G. E. Ozone decomposition. *Interdiscip. Toxicol.* **2014**, *7*, 47–59.

(45) Krapf, M.; El Haddad, I.; Bruns, E. A.; Molteni, U.; Daellenbach, K. R.; Prévôt, A. S. H.; Baltensperger, U.; Dommen, J. Labile Peroxides in Secondary Organic Aerosol. *Chem* **2016**, *1*, 603–616.

(46) Tritscher, T.; Dommen, J.; DeCarlo, P. F.; Gysel, M.; Barmet, P. B.; Praplan, A. P.; Weingartner, E.; Prévôt, A. S. H.; Riipinen, I.; Donahue, N. M.; Baltensperger, U. Volatility and hygroscopicity of aging secondary organic aerosol in a smog chamber. *Atmos. Chem. Phys.* **2011**, *11*, 11477–11496.

(47) Donahue, N. M.; Henry, K. M.; Mentel, T. F.; Kiendler-Scharr, A.; Spindler, C.; Bohn, B.; Brauers, T.; Dorn, H. P.; Fuchs, H.; Tillmann, R.; Wahner, A.; Saathoff, H.; Naumann, K.-H.; Möhler, O.; Leisner, T.; Müller, L.; Reinnig, M.-C.; Hoffmann, T.; Salo, K.; Hallquist, M.; Frosch, M.; Bilde, M.; Tritscher, T.; Barmet, P.; Praplan, A. P.; DeCarlo, P. F.; Dommen, J.; Prévôt, A. S. H.; Baltensperger, U. Aging of biogenic secondary organic aerosol via gas-phase OH radical reactions. *Proc. Natl. Acad. Sci. U.S.A.* **2012**, *109*, 13503–13508.

Graphical TOC Entry

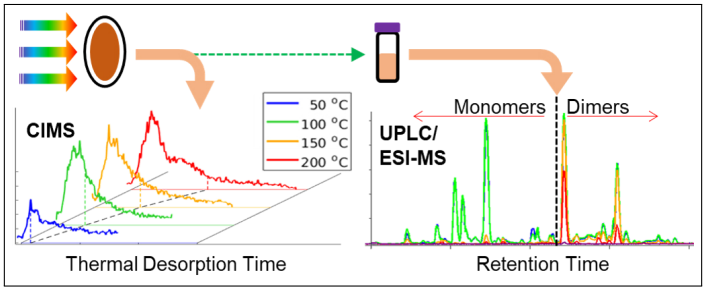

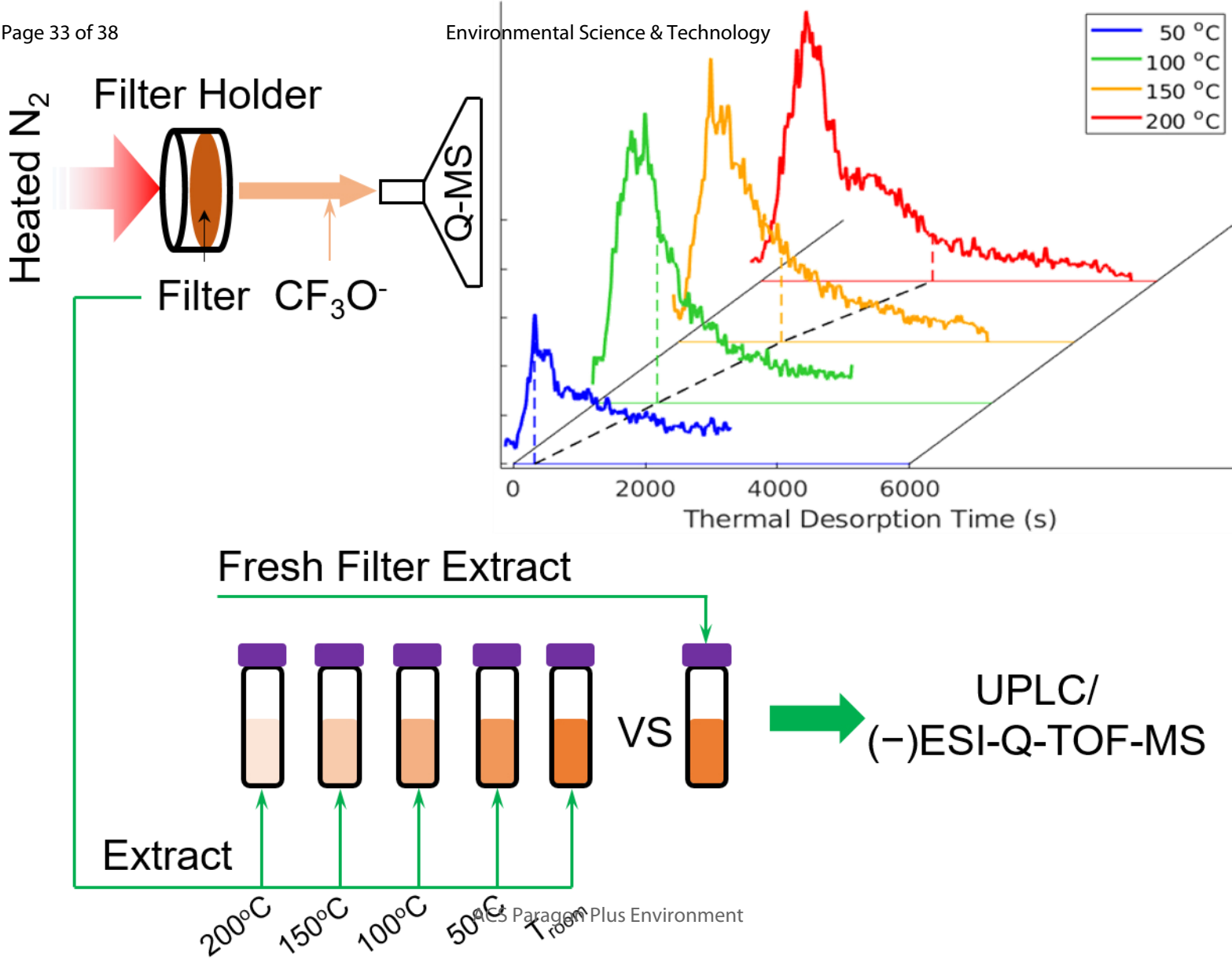
Heated N_2
Filter Holder
Q-MS
Filter
CF_3O^-
50 °C
100 °C
150 °C
200 °C
0
2000
4000
6000
Thermal Desorption Time (s)
Fresh Filter Extract
VS
UPLC/
(−)ESI-Q-TOF-MS
Extract
200°C
150°C
100°C
50°C
T_{room}

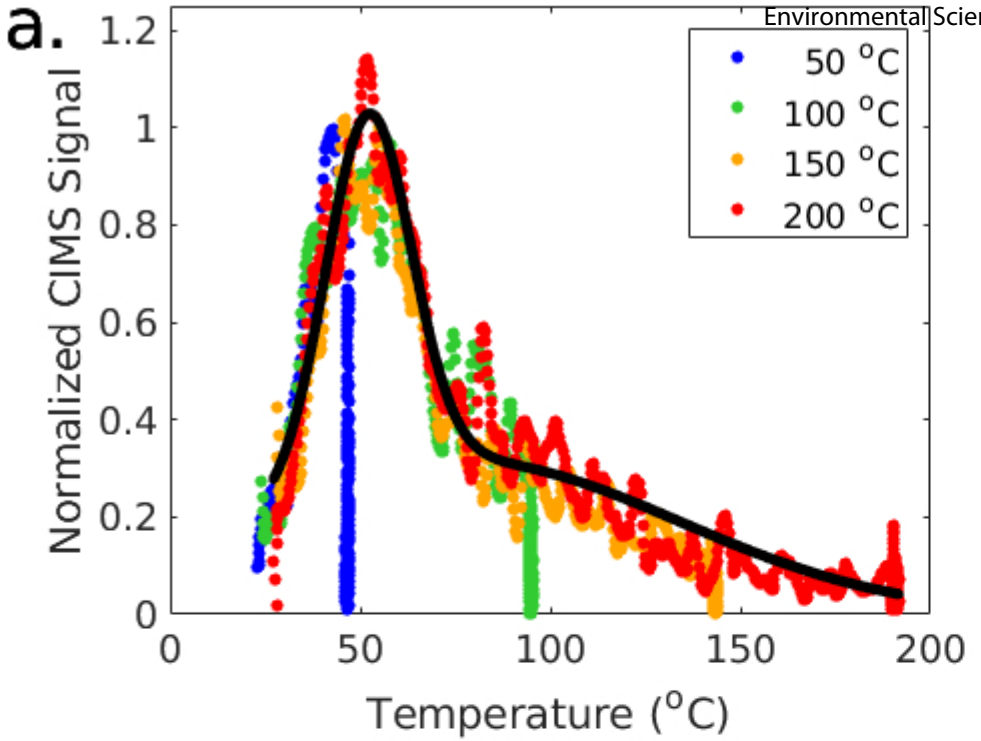
a.
Normalized CIMS Signal
Temperature (°C)
50 °C
100 °C
150 °C
200 °C

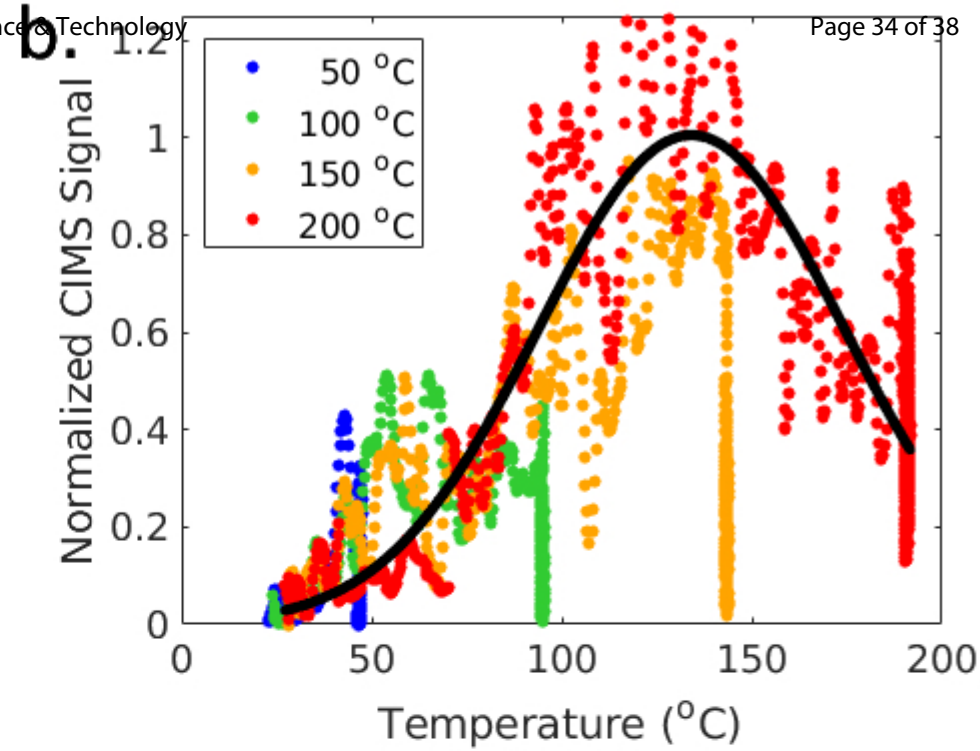
b.
Normalized CIMS Signal
Temperature (°C)
50 °C
100 °C
150 °C
200 °C

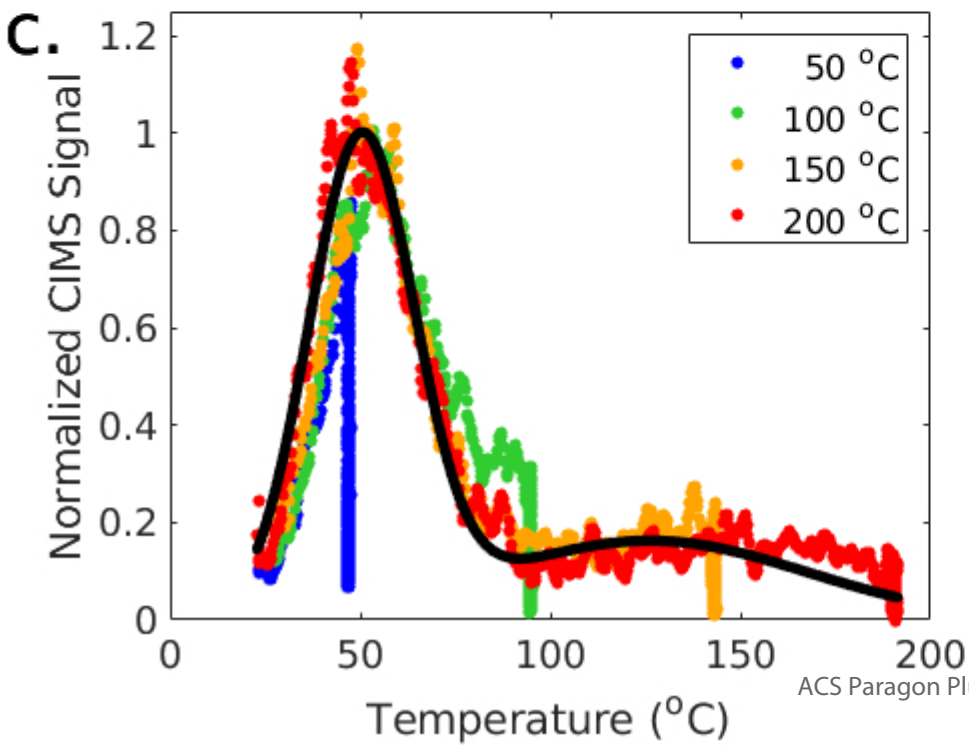
c.
Normalized CIMS Signal
Temperature (°C)
50 °C
100 °C
150 °C
200 °C

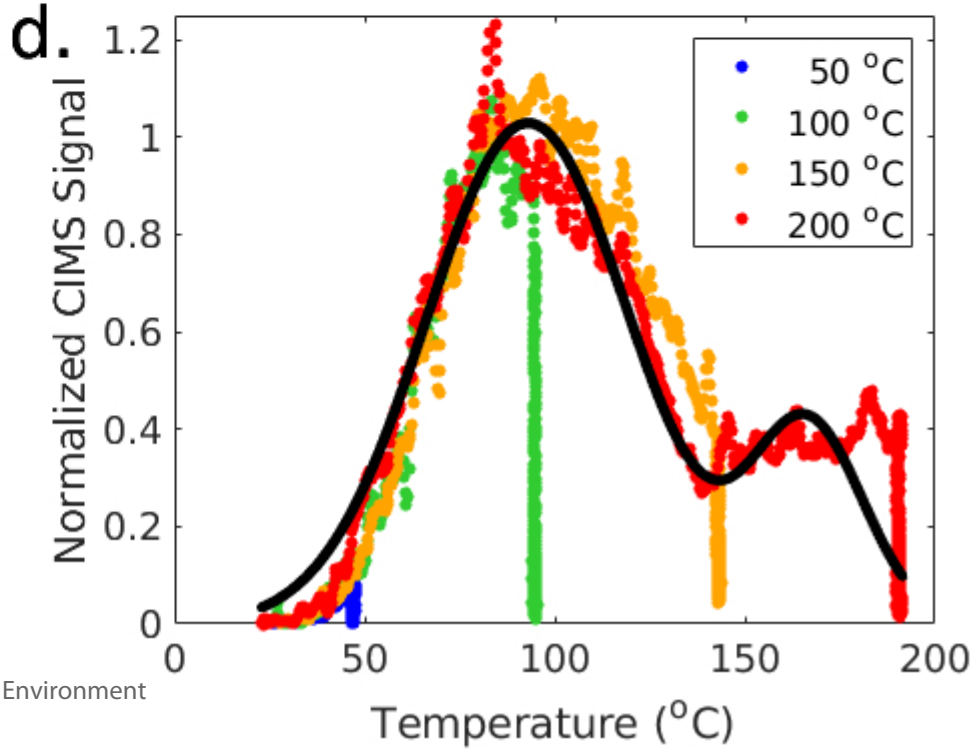
d.
Normalized CIMS Signal
Temperature (°C)
50 °C
100 °C
150 °C
200 °C

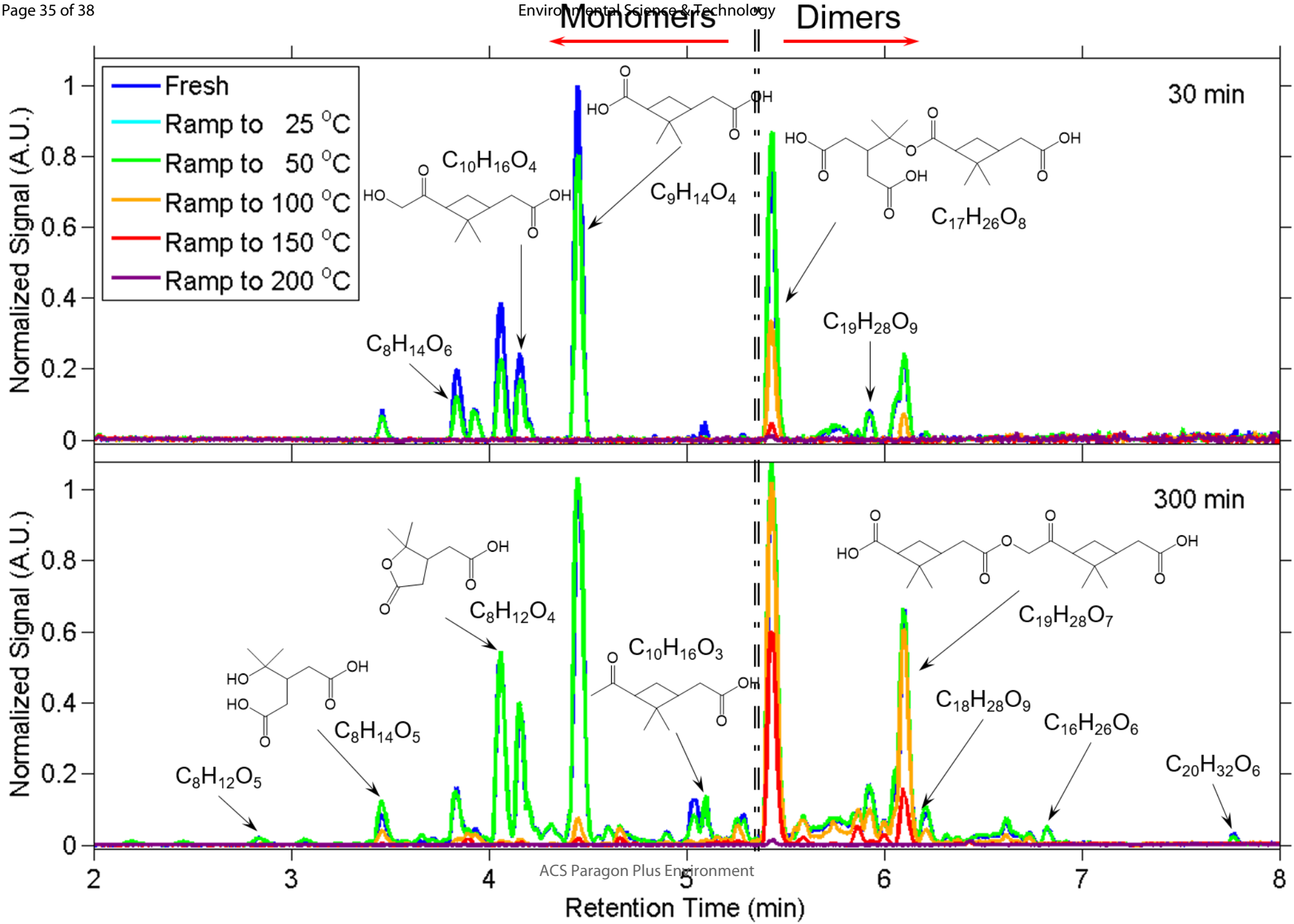

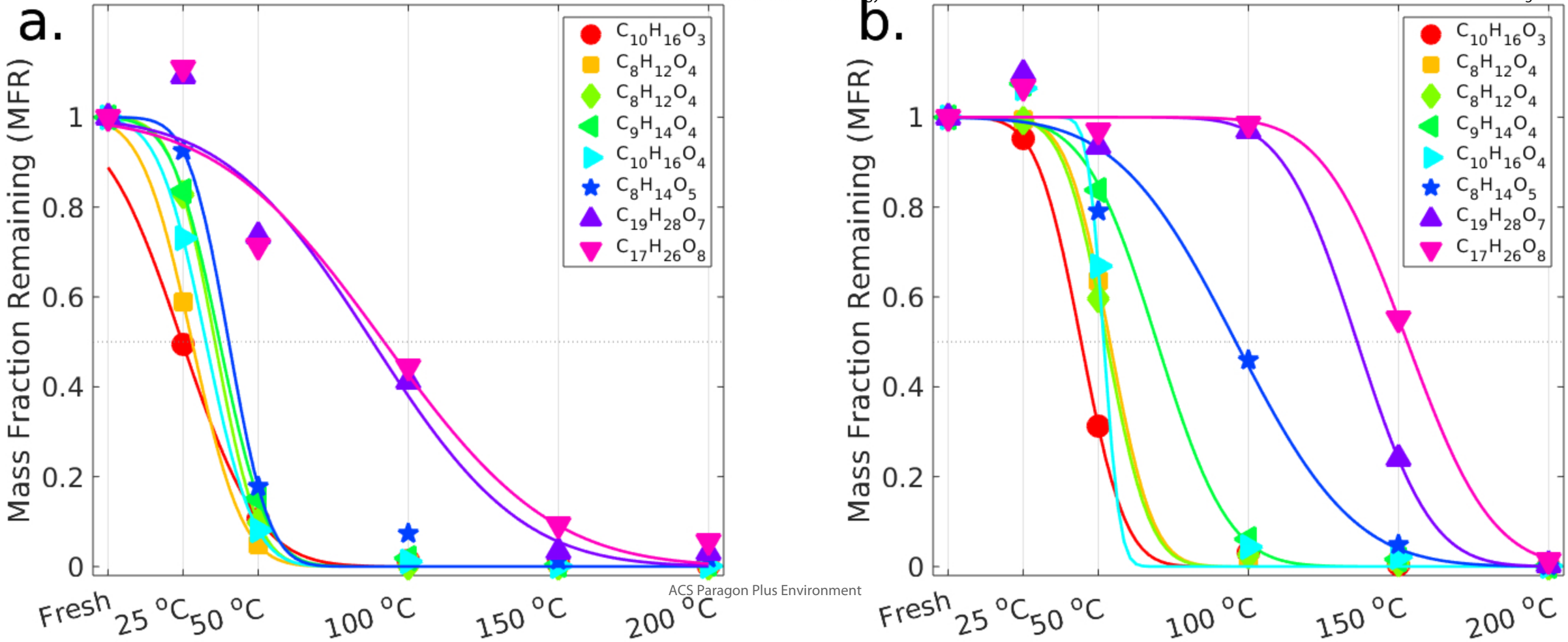
a.
b.
Mass Fraction Remaining (MFR)
0
0.2
0.4
0.6
0.8
1
Fresh
25 °C
50 °C
100 °C
150 °C
200 °C
$C_{10}H_{16}O_3$
$C_8H_{12}O_4$
$C_8H_{12}O_4$
$C_9H_{14}O_4$
$C_{10}H_{16}O_4$
$C_8H_{14}O_5$
$C_{19}H_{28}O_7$
$C_{17}H_{26}O_8$

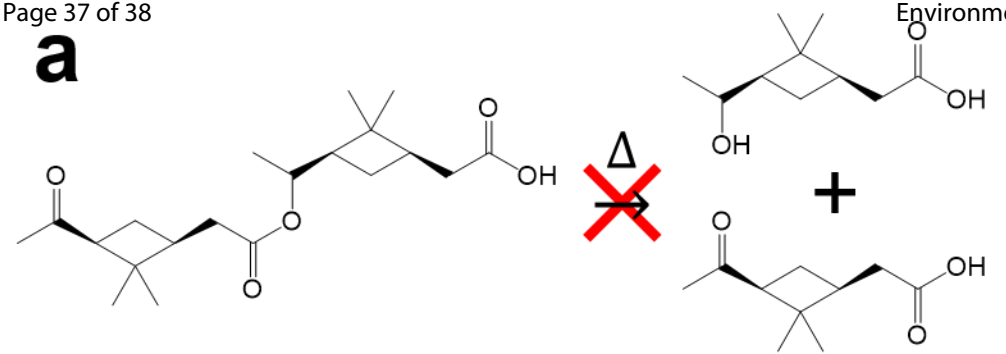
a
OH
OH
OH
OH
Δ

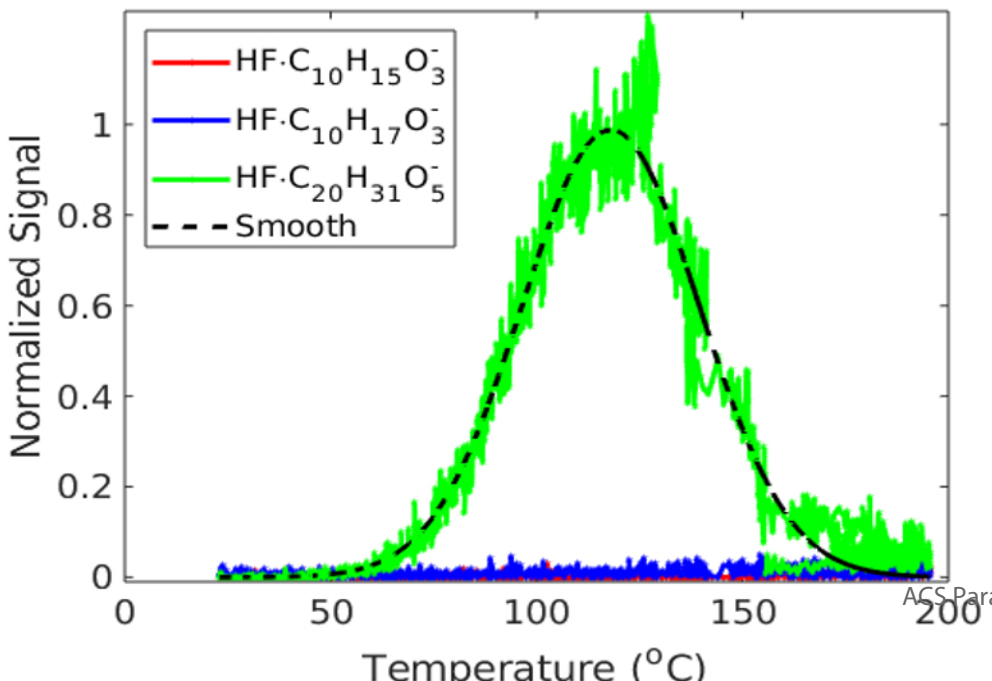
HF·C10H15O3-
HF·C10H17O3-
HF·C20H31O5-
Smooth
Normalized Signal
Temperature (°C)
0
0.2
0.4
0.6
0.8
1
0
50
100
150
200

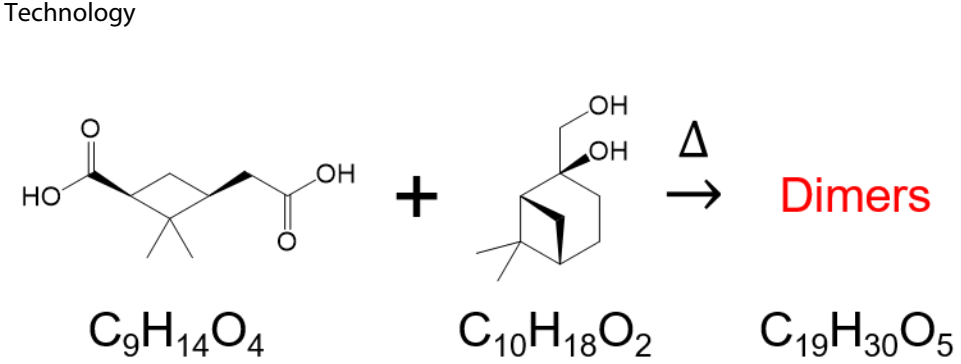
b
HO
OH
OH
OH
Δ
Dimers
C9H14O4
C10H18O2
C19H30O5

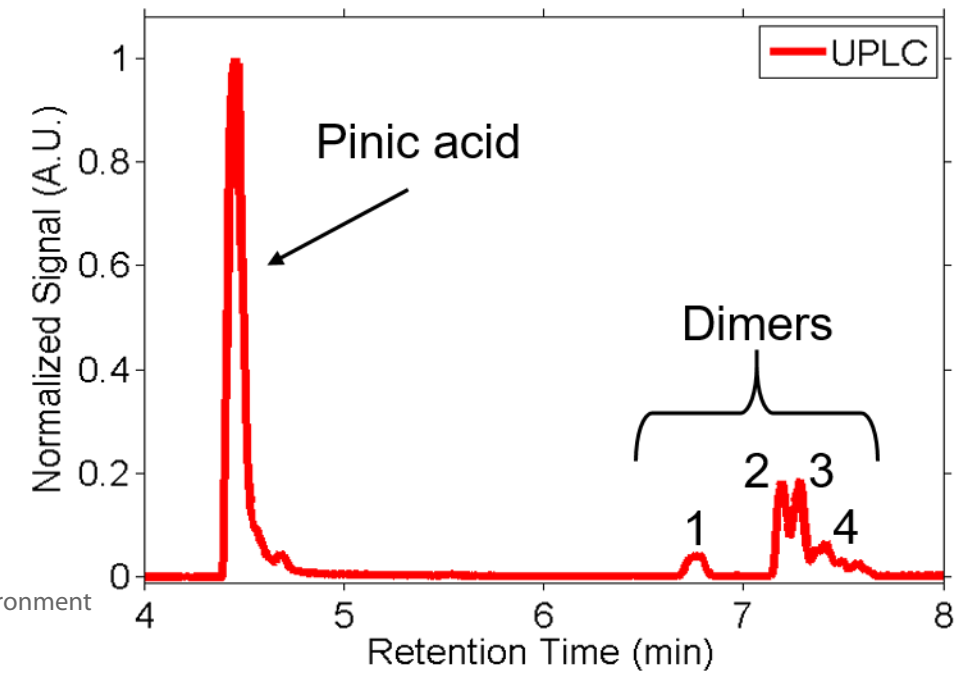
UPLC
Pinic acid
Dimers
1
2
3
4
Normalized Signal (A.U.)
Retention Time (min)
0
0.2
0.4
0.6
0.8
1
4
5
6
7
8